An Improved Fundamental Harmonic Approximation to Describe Filter Inductor Influence on Steady-State Performance of Parallel-Type Resonant Converter

Yiming Chen, Jianping Xu, *Member, IEEE*, Jin Sha, Leiming Lin, and Jing Cao

***Abstract*—The influence of a filter inductor on the steady-state performance of a parallel-type resonant converter is elaborated and analyzed in this paper. By steady-state operation analysis, it is shown that the ripple current of the filter inductor results in an inaccurate prediction of fundamental harmonic approximation (FHA), and such problem would become serious when the filter inductance is small. In order to portray such feature, an improved fundamental harmonic approximation (IFHA) is proposed. Unlike an FHA equivalent circuit, an equivalent inductor is added to the ac resistance parallelly in an IFHA equivalent circuit. Due to that, the equivalent inductor branch takes account of the ripple current of the filter inductor, and the IFHA is expected to own higher accuracy and can be used in a parameter design procedure. In this paper, the equivalent inductor expressions of full-bridge rectifier and current-doubler rectifier are derived as examples. In order to verify the theoretical analysis, a 500 W *LCC* resonant converter is built as a prototype. The close-loop experiment results show that small filter inductance would lead to the failure of output voltage regulation and hard-switching operation of power switches. And open-loop experiment results show the IFHA gives more accurate predictions than those of FHA.**

***Index Terms*—Current-doubler (CD) rectifier, full-bridge (FB) rectifier, filter inductor influence, improved fundamental harmonic approximation (IFHA), parallel-type resonant converter.**

I. Introduction

DURING the past several decades, the benefits of wide soft-switching operation and low electromagnetic interference (EMI) lead to the prosperous development of a resonant converter [1]–[12]. According to the structure of a resonant tank, resonant converters can be categorized into many classifications [1], [2], such as series resonant converter (SRC) [3], parallel resonant converter (PRC) [4], *LCC* [5], *LLC* [6], *LCL* [7], *CLLC* [8] resonant converters, and so on. Usually, such various resonant converters are used in different applications with high requirement of efficiency and full utilization of transformer parasitic parameters.

Manuscript received December 30, 2017; revised March 11, 2018 and May 13, 2018; accepted June 4, 2018. Date of publication June 14, 2018; date of current version February 5, 2019. Recommended for publication by Associate Editor S. K. Mishra. *(Corresponding author: Jianping Xu.)*

The authors are with the School of Electrical Engineering, Southwest Jiaotong University, Chengdu 611756, China, and also with the Key Laboratory of Magnetic Suspension Technology and Maglev Vehicle, Ministry of Education, Chengdu 611756, China (e-mail:

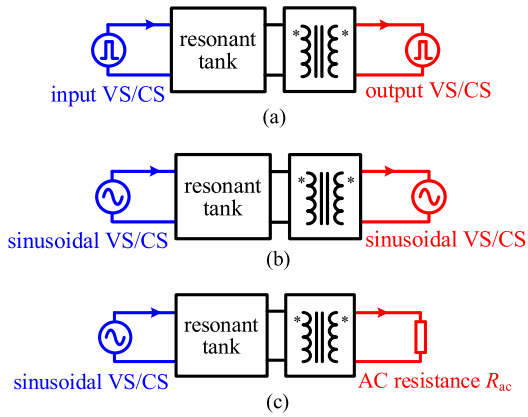

Fig. 1. Process of fundamental harmonic approximation (FHA). (a) Simplified circuit by using square waveform assumption. (b) Equivalent linear circuit with fundamental harmonic components. (c) FHA equivalent circuit with the ac resistance.

For the analysis of resonant converters, fundamental harmonic approximation (FHA) is widely used [9]–[12]. In FHA, it is assumed that only the fundamental harmonic components of current/voltage in the resonant converter have contributions to energy transmission, and thus, the dc and higher order harmonic components of voltage/current in the resonant converter are all ignored due to the orthogonality of the trigonometric function [9]. An illustration of an FHA modeling process is shown in Fig. 1. The first step of FHA is to simplify the circuit of resonant converters, as shown in Fig. 1(a), where the input of the resonant tank and secondary circuit of the transformer are both equivalent to square voltage source (VS) or current source (CS). We define such process as square waveform assumption. Then, by ignoring dc and higher harmonic components of voltage/current in a system, the converter is equivalent to a linear circuit, as shown in Fig. 1(b). Finally, based on the relationship of voltage and current in a rectifier, the secondary circuit of the transformer can be equivalent to the ac resistance R_{ac}, as shown in Fig. 1(c) [9]. The circuit in Fig. 1(c) is also called an FHA equivalent circuit and is widely used in many fields.

Despite FHA achieving success in many occasions, its accuracy is limited. Such issue seriously obstructs the optimization of the converter [13], [14], especially for some duty ratio or phase-shift controlled resonant converters [15]–[21]. Some researchers have pointed out that the deviation between FHA predictions and

practical results comes from the ignorance of high-order harmonic components [16], [22], [23]; hence, time-domain analysis or some extended FHA modeling methods with the information of high-order harmonic components is adopted to solve such problem [19]–[21], [24]–[26]. However, such methods more or less require complex calculation or numerical computation.

Although the ignorance of harmonic components reduces the accuracy of FHA, few second thoughts on the square waveform assumption are paid. For most resonant converters, the existence of input capacitor and primary inverter circuit usually guarantees the input voltage waveform of the resonant tank is square, as shown in Fig. 1(a). However, for the secondary circuit of the transformer, things become different. According to the difference of the resonant tank, capacitive filter or *LC* filter can be used [27], [28]. For some resonant converters like SRC or *LLC*, the capacitive filter is usually adopted. And due to the large filter capacitance and the current-type stimulation of the resonant tank [2], the square secondary voltage waveform of the transformer is usually guaranteed [3], [6], [16]. One exception is the converters operating in a discontinuous conduction mode, and [33] provides a modified modeling method, by using the time-domain information of diode current, to improve FHA accuracy in such occasion. For resonant converters like PRC or *LCC* with a resonant capacitor paralleled on the primary of the transformer, which is also called the parallel-type resonant converter [5], both capacitive filter and *LC* filter can be adopted because such resonant tanks belong to voltage-type [2]. It has been shown that the parallel-type resonant converter with a capacitive filter usually does not satisfy the square waveform assumption, and some amended modeling methods of FHA should be used to solve such problem [5], [20], [29]. However, a deep research on the parallel-type resonant converter with an *LC* filter is still lacking today.

In this paper, the parallel-type resonant converter with the *LC* filter is studied. It is demonstrated that such converter fails to satisfy the square waveform assumption due to the current ripple of a filter inductor. In order to portray such feature, an improved fundamental harmonic approximation (IFHA) is proposed. And the IFHA equivalent circuit of the parallel-type resonant converter is given, where an equivalent inductor is paralleled on the ac resistance. As examples, the equivalent inductors of full-bridge (FB) rectifier and current-doubler (CD) rectifier are derived. To verify the correctness of theoretical analysis, a 500 W *LCC* resonant converter with a CD rectifier is built as a prototype. The close-loop experiment results show the filter inductor could seriously affect the system steady-state performance. And the comparison of open-loop experiment results and FHA/IFHA modeling predictions shows the IFHA benefits from higher accuracy. Therefore, the predictions of IFHA are strongly suggested as the guideline in the parameter design procedure of the parallel-type resonant converter with the *LC* filter.

This paper is organized as follows. Section II introduces the influence of the filter inductor on the parallel-type resonant converter, where detailed steady-state operation analysis of FB rectifier and CD rectifier is given. Section III proposes the IFHA, and the elaborated derivations of equivalent inductors of FB rectifier and CD rectifier are derived. In Section IV, a 500 W *LCC* resonant converter is built as a prototype to show the validity of theoretical analysis, and the comparison of experiment results and modeling predictions is given. Finally, some comprehensive conclusions are given in Section V.

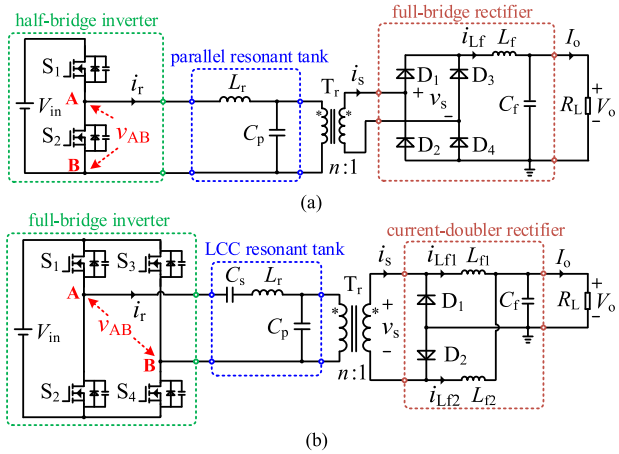

Fig. 2. Two examples of the parallel-type resonant converter. (a) Half-bridge parallel resonant converter with the FB rectifier. (b) Full-bridge LCC resonant converter with the CD rectifier.

II. Influence of the Filter Inductor on the Parallel-Type Resonant Converter

A. Parallel-Type Resonant Converter

Like other resonant converters, the parallel-type resonant converter is composed of inverter, resonant tank, and rectifier. However, the resonant tank in the parallel-type resonant converter requires a parallel capacitor at one side of the transformer. In some applications, such parallel capacitor can be the parasitic capacitance of a power transformer [5], [30]. Fig. 2 illustrates the circuits of two most commonly used parallel-type resonant converters: PRC and *LCC* resonant converter.

As mentioned above, for parallel-type resonant converters, either capacitive or *LC* filter can be used in the secondary circuit of the power transformer. Usually, the capacitive filter is used in high-voltage applications where the volume of the filter inductor can be saved [30], and some kinds of *LC* filters are adopted in low- or medium-voltage applications with small output ripple requirement [28]. This paper focuses on the parallel-type resonant converter with the *LC* filter. For readers interested in the capacitive filter circuit, [5], [20], and [29] are suggested.

In FHA, it is usually assumed that the filter inductance value is large enough, so the filter inductor can be replaced by a constant dc CS for the convenience of analysis [9]. However, we found in some occasions where the filter inductance is not large enough, such assumption brings serious error between modeling predictions and experiment results.

In this section, some elaborated discussions on such issue are given. It should be emphasized that although this paper only discusses the influence of filter inductors in FB rectifier and CD rectifier, a similar analytical method can be easily extended to other rectifiers involving the *LC* filter.

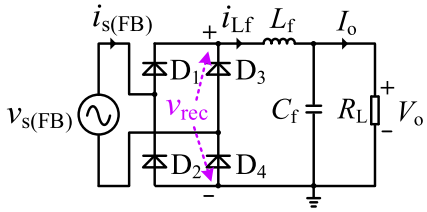

Fig. 3. Equivalent circuit of the parallel-type resonant converter with the FB rectifier.

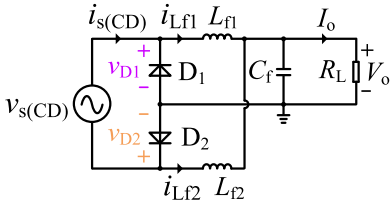

Fig. 5. Equivalent circuit of the parallel-type resonant converter with the CD rectifier.

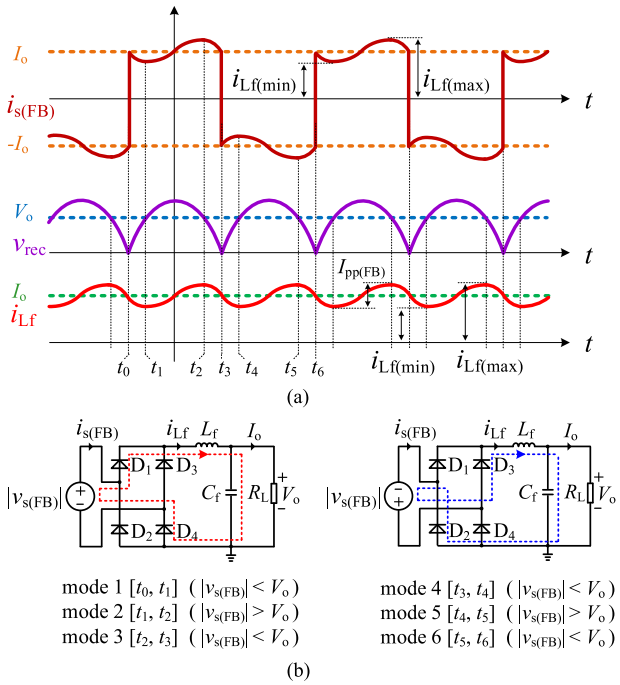

Fig. 4. Key waveforms and equivalent circuits under different operation modes of the parallel-type resonant converter with the FB rectifier. (a) Key waveforms of the parallel-type resonant converter with the FB rectifier. (b) Equivalent circuits of the FB rectifier under different operation modes.

B. Steady-State Operation of a Secondary Rectifier

Among various rectifier circuits, the FB rectifier and CD rectifier are widely used in many applications. By analyzing their steady-state operation, it is shown that the ripple current of the filter inductor in FB rectifier and CD rectifier is very different, which gives an insightful operation principle behind such rectifiers.

1) Parallel-Type Resonant Converter With an FB Rectifier: Due to the frequency-selection characteristic of the resonant tank, the parallel-type resonant converter with the FB rectifier is simplified as the equivalent circuit shown in Fig. 3. In Fig. 3, a sinusoidal voltage source $v_{s(FB)}$ is connected to the input port of the FB rectifier. For the convenience of discussion, we define the input current of the FB rectifier as $i_{s(FB)}$, and the output voltage of the FB rectifier as $v_{rec(FB)}$.

Fig. 4 shows the key waveforms and equivalent circuits under different operation modes of the parallel-type resonant converter with the FB rectifier. In Fig. 4(a), $i_{s(FB)}$ is not a standard square waveform, and the waveform deviation mainly comes from the ripple current of inductor L_f. We define the peak-to-peak current of such ripple current as $I_{pp(FB)}$, as shown in Fig. 4(a). Another important feature of the FB rectifier is the period of $v_{rec(FB)}$ is half of the period of $v_{s(FB)}$; hence, a natural frequency-doubling effect is achieved in the *LC* filter.

From Fig. 4(b), it can be known that diodes D_1 and D_4 are conducted from mode 1 to mode 3, and D_2 and D_3 are conducted from mode 4 to mode 6. For such operation modes, when $|v_{s(FB)}| < V_o$, the current of the filter inductor decreases, and when $|v_{s(FB)}| > V_o$, the current of the filter inductor increases. Given the frequency-doubling effect of $v_{rec(FB)}$, the period of i_{Lf} is also half of the period of $v_{s(FB)}$.

2) Parallel-Type Resonant Converter With a CD Rectifier: Being similar to Fig. 3, due to the frequency-selection characteristic of the resonant tank, the parallel-type resonant converter with the CD rectifier is simplified as the equivalent circuit shown in Fig. 5. In Fig. 5, a sinusoidal voltage source $v_{s(CD)}$ is connected to the input port of the CD rectifier. For the convenience of discussion, we define the input current of the CD rectifier as $i_{s(CD)}$, and the voltage of D_1 and D_2 as v_{D1} and v_{D2}, respectively.

Fig. 6 shows the key waveforms and equivalent circuits under different operation modes of the parallel-type resonant converter with the CD rectifier. From Fig. 6(a), it is noted that $i_{s(CD)}$ is not a standard square waveform, and the waveform deviation mainly comes from the ripple current of inductors L_{f1} and L_{f2}, which are defined as i_{Lf1} and i_{Lf2}, respectively. For the CD rectifier, it is usually guaranteed that $L_{f1} = L_{f2}$; thus, the shapes of i_{Lf1} and i_{Lf2} are identical. We define the peak-to-peak current of i_{Lf1} current as $I_{pp(CD)}$, as shown in Fig. 6(a).

From Fig. 6(b), it can be known that diode D_2 is conducted from mode 1 to mode 3, and i_{Lf1} decreases when $|v_{s(CD)}| < V_o$, and i_{Lf1} increases when $|v_{s(CD)}| > V_o$. It is also noted in such duration, the voltage of L_{f2} is clamped to $-V_o$; thus, i_{Lf2} decreases linearly. Similarly, diode D_1 is conducted from mode 4 to mode 6, and i_{Lf2} decreases when $|v_{s(CD)}| < V_o$, and i_{Lf2} increases when $|v_{s(CD)}| > V_o$. In such duration, the voltage of L_{f1} is clamped to $-V_o$; thus, i_{Lf1} decreases linearly.

i_{Lf1} in the CD rectifier depends on v_{D1} and V_o, and v_{D1} is nonzero only when $v_{s(CD)}$ is positive. Likewise, i_{Lf2} in the CD rectifier depends on v_{D2} and V_o, and v_{D2} is nonzero only when $v_{s(CD)}$ is negative. Due to that no frequency-doubling effect exists in v_{D1} and v_{D2}, the period of i_{Lf1} is the same as that of $v_{s(CD)}$, and so does i_{Lf2}.

By comparing Fig. 4 with Fig. 6, it is concluded that due to the existence of the ripple current on the filter inductor(s), the input current of both FB rectifier and CD rectifier is deviated from the

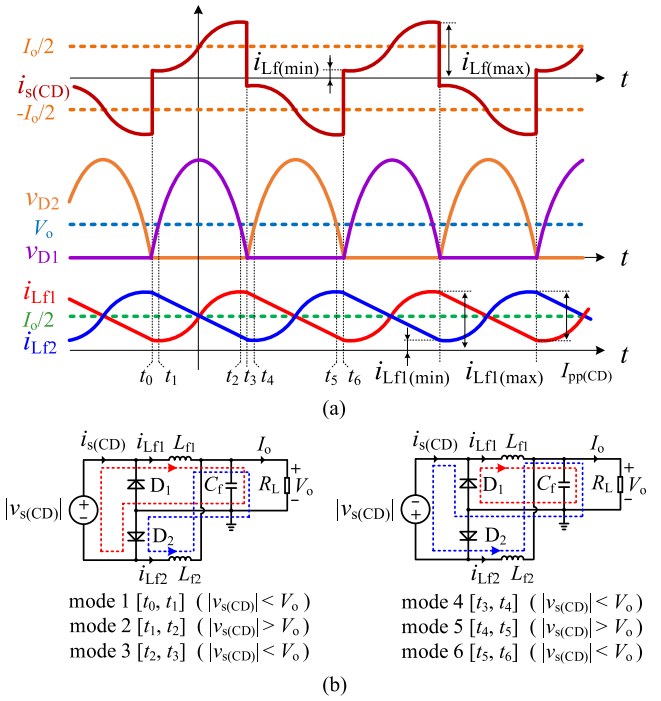

Fig. 6. Key waveforms and equivalent circuits under different operation modes of the parallel-type resonant converter with the CD rectifier. (a) Key waveforms of the parallel-type resonant converter with the CD rectifier. (b) Equivalent circuits of the CD rectifier under different operation modes.

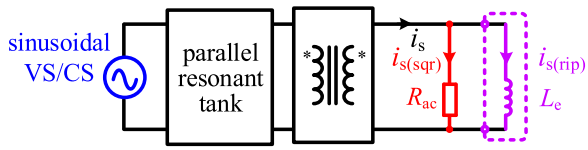

Fig. 7. IFHA equivalent circuit of the parallel-type resonant converter with the *LC* filter.

square waveform. Although FB rectifier and CD rectifier share the same problem, their operation modes are different. In the FB rectifier, due to the frequency-doubling effect of $v_{rec(FB)}$, the frequency of the ripple current on the filter inductor is twice of switching frequency. And in the CD rectifier, the frequency of the ripple current on filter inductors is identical to switching frequency. Such subtle difference leads to different derivations in modeling, which will be discussed in the next section.

III. Experimental Verification

A. Principle of IFHA

Given the square waveform assumptions in FHA, it is expected that such modeling method fails to predict the influence of the filter inductor in the parallel-type resonant converter. In this section, an IFHA is proposed to solve such problem.

Fig. 7 shows the IFHA equivalent circuit of the parallel-type resonant converter. The only difference of IFHA equivalent circuit and FHA equivalent circuit is that there is an equivalent inductor L_e paralleled on R_{ac}. We define the current flowing through R_{ac} as $i_{s(sqr)}$, and the current flowing through L_e as

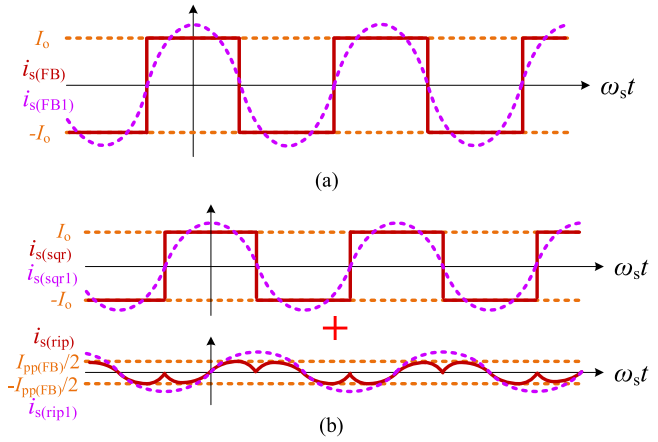

Fig. 8. Key waveforms of the parallel-type resonant converter with the FB rectifier under different modeling methods. (a) Key waveforms under FHA. (b) Key waveforms under IFHA.

$i_{s(rip)}$. By superposition principle, the secondary current of transformer i_s equals the sum of $i_{s(sqr)}$ and $i_{s(rip)}$. Like the FHA method, the current $i_{s(sqr)}$ is the fundamental component of the square output current. However, the current $i_{s(rip)}$ in Fig. 7 introduces the information of the ripple current on the filter inductor; hence, the IFHA is expected to have a higher accuracy.

The key issue of IFHA is how to estimate the value of L_e. In the following derivation, it will be proved that L_e is only relevant to the filter inductor value and rectifier circuit structure, but irrelevant to other circuit parameters, which means the calculation results of L_e can be conveniently extended to parallel-type resonant converters with the same rectifier.

Considering FB rectifier and CD rectifier are widely used in many industrial applications, the elaborated derivation of L_e of FB rectifier and CD rectifier is given as examples. The method can be easily applied to other rectifier circuits with the *LC* filter.

B. Equivalent Inductor of the FB Rectifier

Fig. 8 shows the key waveforms of the parallel-type resonant converter with the FB rectifier under different modeling methods. Fig. 8(a) shows the key waveforms under FHA, where $i_{s(FB)}$ is treated as a square waveform with the amplitude of I_o. And in FHA, only the fundamental harmonic component of $i_{s(FB)}$, defined as $i_{s(FB1)}$, is used. As the above-mentioned explanation, such treatment loses the information of ripple current caused by the filter inductor. Fig. 8(b) shows the key waveforms under IFHA, where $i_{s(sqr)}$ is identical to the $i_{s(FB)}$ in Fig. 8(a), and $i_{s(sqr1)}$ is the fundamental harmonic component of $i_{s(sqr)}$. Unlike FHA, $i_{s(rip)}$ in Fig. 8(b) takes account of the ripple current of the filter inductor. It is noted that due to the rectification of the FB rectifier, $i_{s(rip)}$ is piecewise sinusoidal, and $i_{s(rip1)}$ is defined as the fundamental harmonic component of $i_{s(rip)}$.

According to the volt-second balance of L_f in the FB rectifier, the voltage $v_{s(FB)}$ in Fig. 4 can be expressed as [9]

$$v_{s(FB)} = \frac{\pi V_o}{2}\cos(\omega_s t) \tag{1}$$

where $\omega_s = 2\pi f_s$ is the switching angular frequency. Furthermore, due to the rectification of the FB rectifier, the voltage $v_{\text{rec(FB)}}$ can be expressed as

$$v_{\text{rec(FB)}} = \frac{\pi V_o}{2} \left|\cos\left(\omega_s t\right)\right|. \tag{2}$$

Using Fourier expansion, $v_{\text{rec(FB)}}$ can be written in series as

$$v_{\text{rec(FB)}} = V_o + \sum_{n=2,4,6,\ldots}^{+\infty} \frac{2V_o\cos(n\pi/2)}{(1-n^2)}\cos(n\omega_s t). \tag{3}$$

In IFHA, we omit high-order harmonic components and only use the second harmonic component of $v_{\text{rec(FB)}}$, defined as $v_{rec(FB2)}$, namely

$$v_{\text{rec(FB2)}} = \frac{2V_o}{3}\cos(2\omega_s t). \tag{4}$$

Hence, the second harmonic component of i_{Lf} can be solved as

$$i_{Lf}(2) = \frac{V_o}{3\omega_s L_f}\sin(2\omega_s t). \tag{5}$$

Given the rectification, the expression of $i_{s\text{(rip)}}$ is

$$i_{s\text{(rip)}} = \begin{cases} -\dfrac{V_o}{3\omega_s L_f}\sin(2\omega_s t) & -\pi \le \omega_s t \le -\dfrac{\pi}{2} \\ \dfrac{V_o}{3\omega_s L_f}\sin(2\omega_s t) & -\dfrac{\pi}{2} \le \omega_s t \le \dfrac{\pi}{2} \\ -\dfrac{V_o}{3\omega_s L_f}\sin(2\omega_s t) & \dfrac{\pi}{2} \le \omega_s t \le \pi. \end{cases} \tag{6}$$

The fundamental Fourier coefficient of $i_{s\text{(rip)}}$ is

$$\begin{aligned} F(i_{s\text{(rip1)}}) &= \frac{2}{\pi}\int_{-\pi/2}^{\pi/2} \frac{2V_o}{3\omega_s L_f}\sin(2\omega_s t)\sin(\omega_s t)\, d(\omega_s t) \\ &= \frac{8V_o}{9\pi\omega_s L_f}. \end{aligned} \tag{7}$$

Hence, $i_{s(rip1)}$ can be expressed as

$$i_{s\text{(rip1)}} = \frac{8V_o}{9\pi\omega_s L_f}\sin(\omega_s t). \tag{8}$$

According to Fig. 7, the secondary voltage of transformer $v_{s\text{(FB)}}$ equals the voltage drop of L_e. In the FB rectifier, we notate the equivalent inductor as $L_{e\text{(FB)}}$; therefore, it satisfies

$$\left|v_{s\text{(FB)}}\right| = \omega_s L_{e\text{(FB)}} \left|i_{s\text{(rip1)}}\right|. \tag{9}$$

By combining (1), (8), and (9), $L_{e\text{(FB)}}$ can be solved as

$$L_{e\text{(FB)}} = \frac{9\pi^2}{16}L_f \approx 5.55L_f. \tag{10}$$

Usually, it is required to reflect such equivalent inductor to the primary side of the transformer, defined as $L_{\text{ep(FB)}}$, then we have

$$L_{\text{ep(FB)}} \approx 5.55n^2 L_f. \tag{11}$$

So far, the equivalent inductor of the FB rectifier in IFHA is solved. For a specific parallel-type resonant converter with the FB rectifier, using (11) and the IFHA equivalent circuit in Fig. 7, the system steady-state characteristics can be easily analyzed. The influence of the filter inductor in the circuit is taken into consideration; thus, the error between modeling predictions and experiment results can be greatly reduced. Furthermore, it should be emphasized that such derivation can also apply to a center-tap full-wave rectifier.

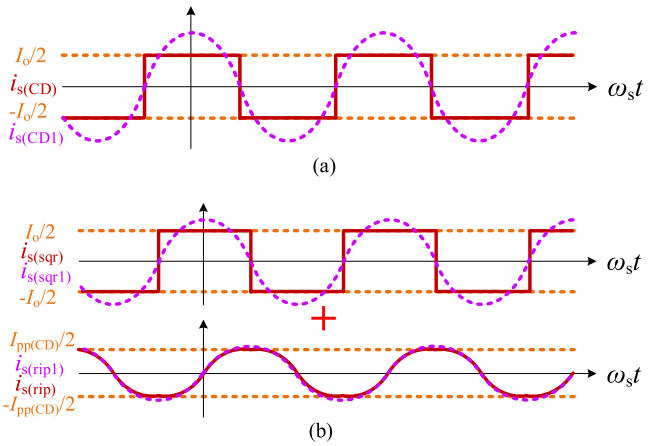

Fig. 9. Key waveforms of the parallel-type resonant converter with the CD rectifier under different modeling methods. (a) Key waveforms under FHA. (b) Key waveforms under IFHA.

C. Equivalent Inductor of the CD Rectifier

Fig. 9 shows the key waveforms of the parallel-type resonant converter with the CD rectifier under different modeling methods. Fig. 9(a) shows the key waveforms under FHA, where $i_{s\text{(CD)}}$ is treated as a square waveform with the amplitude of $I_o/2$. And in FHA, only the fundamental harmonic component of $i_{s\text{(CD)}}$, defined as $i_{s(CD1)}$, is used. As foregoing explanation, such treatment loses the information of the ripple current caused by L_{f1} and L_{f2}. Fig. 9(b) shows the key waveforms under IFHA, where $i_{s\text{(sqr)}}$ is identical to $i_{s\text{(CD)}}$ in Fig. 9(a), and $i_{s(sqr1)}$ is the fundamental harmonic component of $i_{s\text{(sqr)}}$. Unlike FHA, $i_{s\text{(rip)}}$ in Fig. 9(b) takes account of the ripple current of both L_{f1} and L_{f2}. It is noted that due to the rectification of the CD rectifier, $i_{s\text{(rip)}}$ is also piecewise sinusoidal, and $i_{s\text{(rip1)}}$ is defined as the fundamental harmonic component of $i_{s\text{(rip)}}$.

According to the volt-second balance of L_{f1} in the CD rectifier, the voltage $v_{s\text{(CD)}}$ in Fig. 6 can be expressed as [9]

$$v_{s\text{(CD)}} = \pi V_o \cos\left(\omega_s t\right). \tag{12}$$

Given the rectification of the CD rectifier, the voltage v_{D1} can be expressed as

$$v_{D1} = \begin{cases} 0 & -\pi \le \omega_s t \le -\pi/2 \\ \pi V_o\cos\left(\omega_s t\right) & -\pi/2 \le \omega_s t \le \pi/2 \\ 0 & \pi/2 \le \omega_s t \le \pi. \end{cases} \tag{13}$$

Using Fourier expansion, v_{D1} can be written in series as

$$v_{D1} = V_o + \frac{\pi V_o}{2}\cos(\omega_s t) + \sum_{n=2,4,6,\ldots}^{+\infty} \frac{2V_o\cos(n\pi/2)}{(1-n^2)}\cos(n\omega_s t). \tag{14}$$

Although we can use the similar method as in the FB rectifier, neither fundamental nor second harmonic component of v_{D1} is recommended to be used here; this is because such components are

$$v_{D1(1)} = \frac{\pi V_o}{2}\cos(\omega_s t) \tag{15}$$

$$v_{D1(2)} = \frac{2V_o}{3}\cos(2\omega_s t). \tag{16}$$

It can be seen that the magnitudes of $v_{D1(1)}$ and $v_{D1(2)}$ are very close. Neglecting anyone of them would introduce serious error in the modeling. If both components are taken into consideration, it would lead to a complex expression of the equivalent inductor. Fortunately, according to Fig. 9(b), it is noted that the waveforms of $i_{s(\mathrm{rip1})}$ and $i_{s(\mathrm{rip})}$ are very close. Hence, it is reasonable to assume $i_{s(\mathrm{rip1})} \approx i_{s(\mathrm{rip})}$, which means the peak-to-peak current of $i_{s(\mathrm{rip1})}$ is approximate to $I_{\mathrm{pp(CD)}}$. And according to Fig. 6(a), $I_{\mathrm{pp(CD)}}$ can be estimated as

$$I_{\mathrm{pp(CD)}} \approx \frac{\pi V_o}{\omega_s L_{f1}}. \tag{17}$$

Therefore, the expression of $i_{s(\mathrm{rip1})}$ is

$$is(\mathrm{rip1}) \approx \frac{I_{\mathrm{pp(CD)}}}{2}\sin(\omega_s t) = \frac{\pi V_o}{2\omega_s L_{f1}}\sin(\omega_s t). \tag{18}$$

According to Fig. 7, the secondary voltage of transformer $v_{s(\mathrm{CD})}$ equals the voltage drop of L_e. In the CD rectifier, we notate the equivalent inductor as $L_{e(\mathrm{CD})}$; therefore, it satisfies

$$|v_{s(\mathrm{CD})}| = \omega_s L_{e(\mathrm{CD})}\,|i_{\mathrm{rip(CD1)}}|\,. \tag{19}$$

By combining (12), (18), and (19), $L_{e(\mathrm{CD})}$ can be solved as

$$L_{e(\mathrm{CD})} = 2L_{f1}. \tag{20}$$

Usually, it is required to reflect such equivalent inductor to the primary side of the transformer, defined as $L_{\mathrm{ep(CD)}}$, then we have

$$L_{\mathrm{ep(CD)}} = 2n^2 L_{f1}. \tag{21}$$

Thus far, the equivalent inductor of the CD rectifier in IFHA is solved. For a specific parallel-type resonant converter with the CD rectifier, using (21) and the IFHA equivalent circuit in Fig. 7, the system steady-state characteristics can be easily analyzed. Since the influence of the filter inductor in the circuit is taken into consideration, the IFHA is expected to provide more accurate steady-state analysis results than FHA.

IV. Example of the Parallel-Type Resonant Converter

For the sake of verifying the theoretical analysis and the accuracy of IFHA, an *LCC* resonant converter with the CD rectifier is built as an example. The steady-state characteristics of the *LCC* resonant converter are analyzed, by FHA and IFHA. The close-loop and open-loop experiment results are measured with different filter inductor values. The comparison of theoretical analysis and experiment results is given in this section.

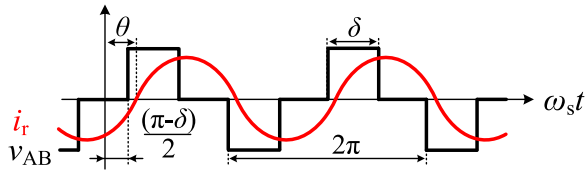

Fig. 10. Steady-state waveforms of the *LCC* resonant converter.

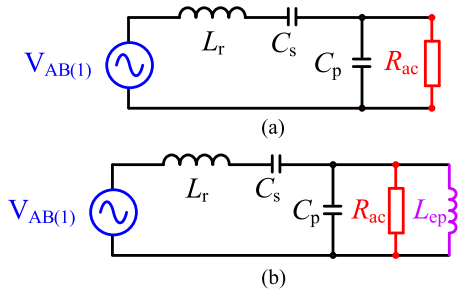

Fig. 11. Equivalent circuit of the *LCC* resonant converter with the CD rectifier under different modeling methods. (a) FHA equivalent circuit of the *LCC* resonant converter. (b) IFHA equivalent circuit of the *LCC* resonant converter.

A. Steady-State Analysis of the LCC Resonant Converter

The circuit of the *LCC* resonant converter with the CD rectifier is shown in Fig. 2(b), and its steady-state waveforms are illustrated in Fig. 10. δ in Fig. 10 is a conduction angle [31], and θ is the input impedance angle of the resonant converter.

The zero voltage switching (ZVS) condition of the *LCC* resonant converter is [31]

$$\theta > \frac{\pi - \delta}{2}. \tag{22}$$

For designers, it is important to make the *LCC* resonant converter satisfy both voltage regulation condition and ZVS condition; thus, a precise steady-state analysis is necessary.

The FHA/IFHA equivalent circuits of the *LCC* resonant converter with the CD rectifier are illustrated in Fig. 11, where $R_{\mathrm{ac}} = (n^2\pi^2 R_L)/2$ [9] and $L_{\mathrm{ep}} = 2n^2 L_{f1}$. It should be mentioned that if the FB rectifier is adopted, the expressions of R_{ac} and L_{ep} should be changed as $R_{\mathrm{ac}} = (n^2\pi^2 R_L)/8$ [9] and $L_{\mathrm{ep}} = 5.55n^2 L_f$ in this instance.

With the FHA equivalent circuit shown in Fig. 11(a), the voltage gain $M_{(\mathrm{FHA})}$ of the LCC resonant converter can be solved as [31]

$$M_{(\mathrm{FHA})} = \frac{V_o}{V_{\mathrm{in}}} = \frac{1}{n} \times \left| \frac{2}{\frac{\pi^2}{2}\left[1 + \frac{C_p}{C_s} - \frac{C_p}{C_s}\left(\frac{\omega_s}{\omega_{sr}}\right)^2\right] + jQ\left[\frac{\omega_s}{\omega_{sr}} - \frac{\omega_{sr}}{\omega_s}\right]} \right| \sin\left(\frac{\delta}{2}\right) \tag{23}$$

where

$$\omega_{sr} = \frac{1}{\sqrt{L_r C_s}}, \quad Q = \frac{1}{n^2 R_L}\sqrt{\frac{L_r}{C_s}} \tag{24}$$

are series resonant angular frequency and quality factor of the *LCC* resonant converter, respectively. Similarly, with Fig. 11(a), the input impedance $Z_{\text{in(FHA)}}$ and impedance angle $\theta_{\text{(FHA)}}$ are

$$Z_{\text{in(FHA)}} = \frac{R_{\text{ac}}}{1+\omega_s^2 C_p^2 R_{\text{ac}}^2} + j\left(\omega_s L_r - \frac{1}{\omega_s C_s} - \frac{\omega_s C_p R_{\text{ac}}^2}{1+\omega_s^2 C_p^2 R_{\text{ac}}^2}\right) \tag{25}$$

$$\theta_{\text{(FHA)}} = \arctan\left[\frac{1+\omega_s^2 C_p^2 R_{\text{ac}}^2}{R_{\text{ac}}} \times \left(\omega_s L_r - \frac{1}{\omega_s C_s} - \frac{\omega_s C_p R_{\text{ac}}^2}{1+\omega_s^2 C_p^2 R_{\text{ac}}^2}\right)\right]. \tag{26}$$

If the IFHA equivalent circuit in Fig. 11(b) is used, the voltage gain $M_{\text{(IFHA)}}$, input impedance $Z_{\text{in(IFHA)}}$, and impedance angle $\theta_{\text{(IFHA)}}$ of the *LCC* resonant converter can be derived as, (27) shown at the bottom of the page

$$Z_{\text{in(IFHA)}} = R_{\text{in(IFHA)}} + jX_{\text{in(IFHA)}} \tag{28}$$

$$\theta_{\text{(IFHA)}} = \arctan\left(\frac{X_{\text{in(IFHA)}}}{R_{\text{in(IFHA)}}}\right) \tag{29}$$

where

$$R_{\text{in(IFHA)}} = \frac{R_{\text{ac}}}{1+\left[\omega_s C_p - 1/(\omega_s L_{\text{ep}})\right]^2 R_{\text{ac}}^2} \tag{30}$$

$$X_{\text{in(IFHA)}} = \omega_s L_r - \frac{1}{\omega_s C_s} - \frac{\left[\omega_s C_p - 1/(\omega_s L_{\text{ep}})\right] R_{\text{ac}}^2}{1+\left[\omega_s C_p - 1/(\omega_s L_{\text{ep}})\right]^2 R_{\text{ac}}^2}. \tag{31}$$

It can be shown that for (27)–(31), when L_{ep} goes to infinity, the results of such equations would be the same as (23)–(26). Therefore, the FHA is a simplified version of IFHA.

In practical applications, on one hand, the filter inductance in the parallel-type resonant converter is usually designed by EMI and output ripple requirements. On the other hand, the value of such inductance would not be very large due to the limitation of system volume. Therefore, when such inductance is small, the difference of IFHA and FHA can be remarkable.

According to (27)–(31), it is evident that the filter inductor not only influences the voltage gain of the *LCC* resonant converter, but also system input impedance and impedance angle. Such phenomena affect the performance of the *LCC* resonant converter in two ways: 1) it may lead to the failure of voltage regulation under some specific operation conditions and 2) it may lead to the failure of ZVS of power switches under some specific operation conditions. The phenomena are proved in the experiment in Section IV-B.

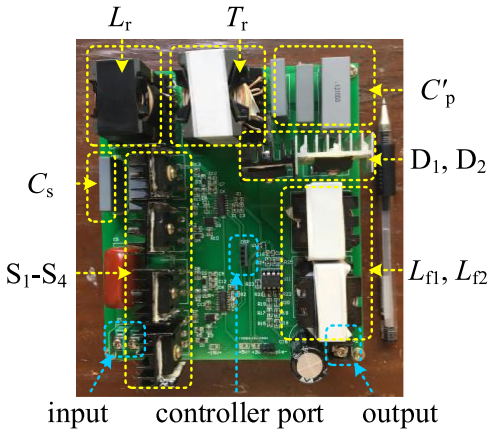

Fig. 12. Photograph of the prototype.

TABLE I
CIRCUIT PARAMETERS FOR THE EXPERIMENT PROTOTYPE

Description	Symbol	Value / Type
Input voltage	V_{in}	100V-200V
Output voltage	V_{o}	48V
Output Power	P_{o}	100W-500W
Resonant inductor	L_{r}	82μH, PQ3230
Series resonant capacitor	C_{s}	2×30nF, CBB111
Parallel resonant capacitor	C'_{p}	(100+30+10)nF, CBB111
Power transformer	T_{r} (n:1)	1.55:1, PQ3535
Filter inductor(s)	L_{f1}, L_{f2}	2×80μH/22μH, EI33
Output capacitor	C_{f}	100μF, 100V, Electrolytic
Power MOSFETs	S_1~S_4	4×SPW47N60CFD
Diodes	D_1, D_2	2×APT30S20BCTG
Control coefficient K	K	1.086e-4
Control coefficient B	B	14.313

It should also be emphasized for the *LCC* resonant converter, the accuracy of FHA is usually good if the system operates under a continuous capacitor voltage mode (CCVM), and FHA would fail if the system operates under a discontinuous capacitor voltage mode (DCVM) [24]. However, in this paper, we only discuss the *LCC* resonant converter operating under the CCVM and prove that even in such situation FHA could result in a large prediction error due to the influence of the filter inductor.

B. Experiment Results of a PWM–PFM Hybrid Controlled LCC Resonant Converter With Different Filter Inductors

In order to show the influence of the filter inductor for the parallel-type resonant converter, an *LCC* resonant converter prototype is built. Fig. 12 shows the implementation of the experiment prototype, and Table I provides the detailed circuit parameters. In the prototype, the parallel resonant capacitor C_p is placed in the secondary side of the transformer with reflected capaci-

$$M_{(IFHA)} = \frac{1}{n}\left|\frac{2}{\frac{\pi^2}{2}\left[1+\frac{C_p}{C_s}-\frac{C_p}{C_s}\left(\frac{\omega_s}{\omega_{sr}}\right)^2+\frac{L_r}{L_{\text{ep}}}-\frac{L_r}{L_{\text{ep}}}\left(\frac{\omega_{sr}}{\omega_s}\right)^2\right]+jQ\left[\frac{\omega_s}{\omega_{sr}}-\frac{\omega_{sr}}{\omega_s}\right]}\right|\sin\left(\frac{\delta}{2}\right) \tag{27}$$

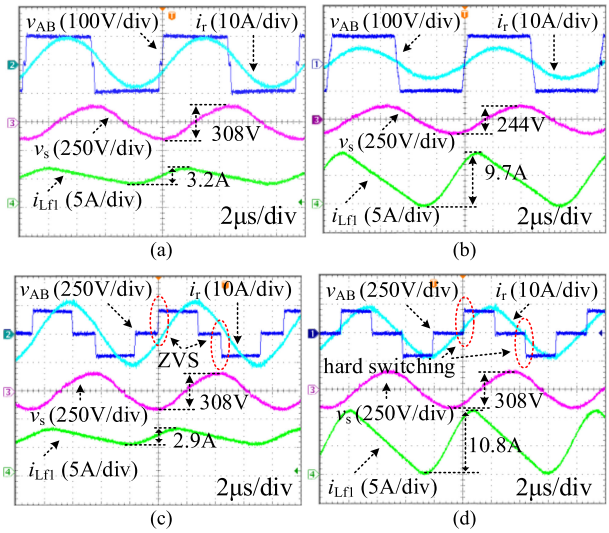

Fig. 13. Experiment waveforms of the prototype with different filter inductors. (a) $V_{\text{in}} = 100$ V, $P_o = 500$ W, $L_f = 80$ μH. (b) $V_{\text{in}} = 100$ V, $P_o = 500$ W, $L_f = 22$ μH. (c) $V_{\text{in}} = 200$ V, $P_o = 100$ W, $L_f = 80$ μH. (d) $V_{\text{in}} = 200$ V, $P_o = 100$ W, $L_f = 22$ μH.

tance C_p'; thus, the leakage inductance of the power transformer can be absorbed into L_r. The control strategy comes from [32], where the conduction angle and switching frequency satisfy

$$f_s = -K\delta + B. \tag{32}$$

Such pulsewidth modulation (PWM)–pulse frequency modulation (PFM) hybrid control strategy can effectively reduce the switching frequency variation of the *LCC* resonant converter without losing wide ZVS operation feature.

The close-loop experiment waveforms of the prototype with different filter inductance are shown in Fig. 13, where the inverter output voltage v_{AB}, resonant current i_r, transformer secondary voltage v_s, and inductor filter current i_{Lf1} are illustrated. From Fig. 13, it can be known that both switching frequency and conduction angle of the *LCC* resonant converter are adjusted, which is the effect of the PWM–PFM hybrid control method as [32].

Fig. 13(a) and (b) shows the waveforms of the prototype under $V_{\text{in}} = 100$ V and $P_o = 500$ W, with 80 and 22 μH filter inductor, respectively. In Fig. 13(a), due to the large filter inductance, the peak-to-peak ripple current of i_{Lf1} is only 3.2 A. And the peak-to-peak voltage of v_s reaches 308 V, which is approximate to $2\pi V_o$, meaning the output voltage of the prototype is regulated [9]. However, Fig. 13(b) shows the peak-to-peak voltage of v_s is only 244 V, meaning the output voltage regulation is failed under such condition. The reason is that the filter inductance is only 22 μH, and it seriously affects the steady-state performance of the prototype. As shown, the peak-to-peak ripple current of i_{Lf1} is as high as 10.7 A under such condition. Meanwhile, it is noted that the sinusoidal waveform of v_s shows the converter operating under the CCVM [24]; hence, the influence does not come from the DCVM operation.

Fig. 13(c) and (d) shows the waveforms of the prototype under $V_{\text{in}} = 200$ V and $P_o = 100$ W, with 80 and 22 μH filter inductor, respectively. As can be observed, the peak-to-peak ripple current of i_{Lf1} is only 2.9 A in Fig. 13(c) due to the large filter inductance. Furthermore, it is noted that the zero-crossing moment of resonant current is later than the turn-ON moment of lagging leg switches in Fig. 13(c), which means all switches operate under ZVS turn-ON operation [31]. However, when the filter inductance reduces to 22 μH, the situation is different under the same operation condition, as shown in Fig. 13(d), where the peak-to-peak ripple current of i_{Lf1} reaches 10.8 A. On the other hand, the turn-ON moment of lagging leg switches is later than the zero-crossing moment of the resonant current, meaning the switches of the lagging leg operate under hard-switching operation. Such hard-switching operation seriously deteriorates system performance: it increases the EMI of the system, voltage stress of power switches, and switching loss of the converter [32]. Similarly, the sinusoidal waveform of v_s shows the converter operating under the CCVM [24]; thus, the influence does not come from the DCVM operation.

Therefore, the filter inductor affects the steady-state performance of the parallel-type resonant converter in two ways: 1) it changes the voltage gain of the converter, leading to the failure of output voltage regulation under some specific conditions and 2) it changes the impedance angle of the converter, resulting in the hard-switching operation of lagging leg switches under some specific conditions. Such potential issues are significant for resonant converters, because they reveal that the benefits of voltage regulation and soft-switching operation might be totally lost due to the influence of the filter inductor.

C. Comparison of Experiment Results and Modeling Results

As mentioned above, the influence of the filter inductor leads to some serious problems for parallel-type resonant converters. Therefore, in the parameter design procedure, it is necessary to take such influence into consideration. The IFHA proposed in this paper is actually the tool for solving such issue. For the *LCC* resonant converter, as shown in Fig. 2(b), it is suggested to use (27)–(31) to calculate the voltage gain and impedance angle instead of (23)–(26) in the parameter design procedure.

To demonstrate the accuracy of IFHA, the open-loop experiment results of the prototype and modeling predictions by FHA/IFHA are given, as shown in Fig. 14, where the detailed model parameters are listed in Table II. The dotted lines in Fig. 14 are the predictions of FHA and the solid lines are the predictions of IFHA, and open-loop experiment results are presented as the discrete dots in Fig. 14. The base frequency in Fig. 14 is series–parallel resonant frequency f_{sp}, which is expressed as

$$f_{\text{sp}} = \frac{1}{2\pi}\sqrt{\frac{C_s + C_p}{L_r C_s C_p}}. \tag{33}$$

In the implementation, such series–parallel resonant frequency is designed as 100 kHz [9].

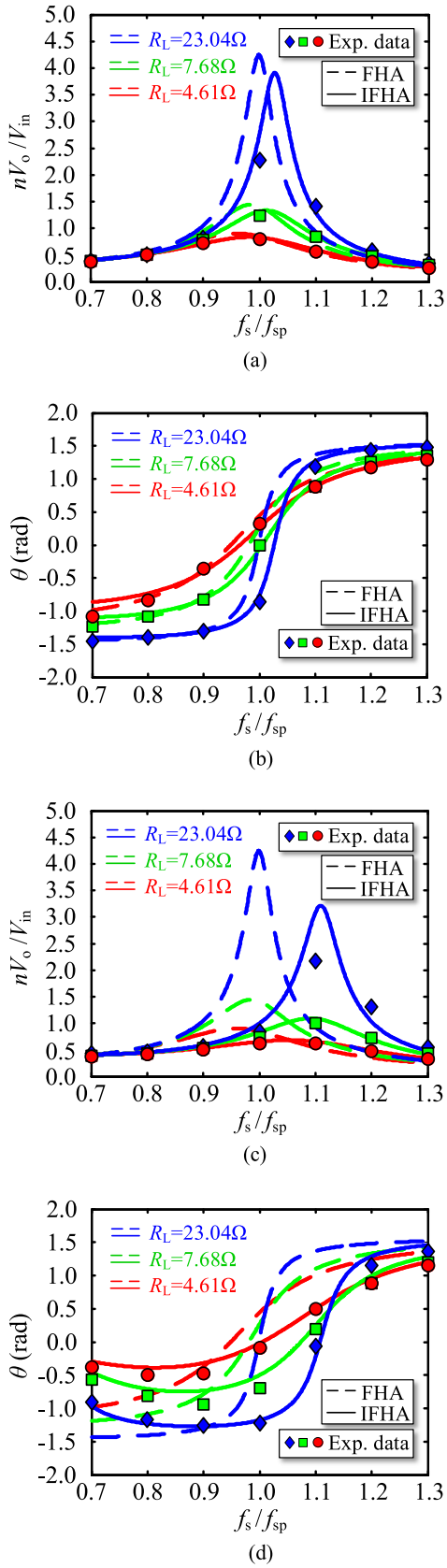

Fig. 14. Comparison of experiment results and modeling predictions. (a) Normalized voltage gain with $L_{f1} = L_{f2} = 80\ \mu$H. (b) Impedance angle with $L_{f1} = L_{f2} = 80\ \mu$H. (c) Normalized voltage gain with $L_{f1} = L_{f2} = 22\ \mu$H. (d) Impedance angle with $L_{f1} = L_{f2} = 22\ \mu$H.

TABLE II
MODEL PARAMETERS IN THE FHA/IFHA EQUIVALENT CIRCUIT

Model Parameters	Symbol	Value
Resonant inductor	L_r	82μH
Series resonant capacitor	C_s	60nF
Parallel resonant capacitor	C_p	60nF
Load resistance	R_L	4.61Ω / 7.68Ω / 23.04Ω
AC resistance	R_{ac}	55.4Ω / 92.2Ω / 276.7Ω
Filter inductance	L_{fl}	22μH / 80μH
Equivalent inductor	L_{ep}	107.1μH / 289.4μH

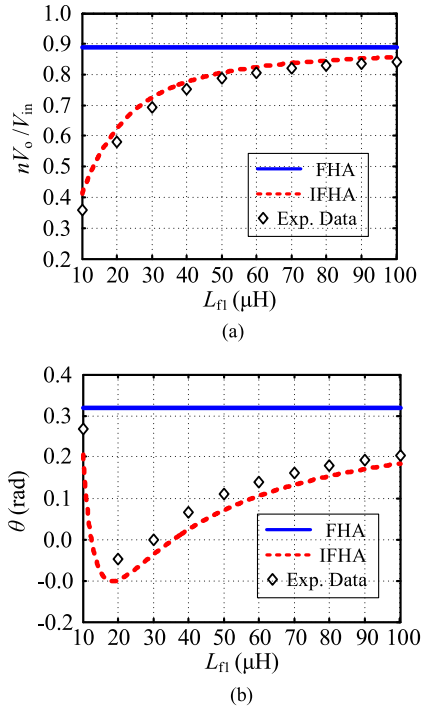

Fig. 15. Relationship of FHA/IFHA predictions and filter inductance (with $f_s = 100$ kHz, $\delta = \pi$). (a) Normalized voltage gain. (b) Impedance angle.

Fig. 14(a) and (b) shows the normalized voltage gain and impedance angle of the prototype under different output loads with $L_{f1} = L_{f2} = 80\ \mu$H. It can be seen that for both voltage gain and impedance angle, the predictions of FHA and IFHA are very close due to the large filter inductance. However, the experiment data are more accordant with the IFHA predictions indeed. In practical applications, because some margin can be added in the parameter design procedure, it is okay to use FHA as the guideline under such condition.

Fig. 14(c) and (d) shows the normalized voltage gain and impedance angle of the prototype under different output loads with $L_{f1} = L_{f2} = 22\ \mu$H. Under such small filter inductance, it can be seen that for both voltage gain and impedance angle, the predictions of FHA and IFHA are very different. Under such condition, compared with the experiment data, only IFHA gives the accurate predictions of steady-state characteristics of the prototype. The predictions of FHA have large deviation, and it is not recommended as the parameter design guideline anymore.

Fig. 15 shows the relationship of FHA/IFHA predictions and filter inductance. It is noted that because the FHA modeling

does not take filter inductance into consideration, the predicted normalized gain and impedance angle are independent of the filter inductance. However, it can be seen that the predicted normalized gain and impedance angle in IFHA are influenced by the filter inductance, and the open-loop experiment data are more accordant with the IFHA predictions. From Fig. 15(a), the predicted normalized gain of IFHA is always lower than that of FHA and it decreases with the decrease of filter inductance. Therefore, the smaller the filter inductance, the greater the error would occur in FHA. Similarly, in Fig. 15(b), the predicted impedance angle of IFHA is always lower than that of FHA, but the maximum error of FHA occurs at $L_{f1} = 20\ \mu$H. In the implementation, we choose $L_{f1} = 22\ \mu$H to illustrate the influence of filter inductance on both normalized gain and impedance angle.

As the conclusion, the IFHA provides a useful tool for designers to predict the influence of the filter inductor in the parallel-type resonant converter. With the help of IFHA modeling, the failure of voltage regulation and soft-switching operation caused by the filter inductor can be avoided.

V. Conclusion

The influence of the filter inductor on the steady-state performance of the parallel-type resonant converter is studied and analyzed in this paper. As examples, the steady-state operation of parallel-type resonant converters with FB rectifier and CD rectifier is elaborated. It is shown that for such converters, the ripple current of the filter inductor deteriorates the accuracy of FHA modeling. In order to solve such problem, an IFHA is proposed in this paper. By paralleling an equivalent inductor on the ac resistance, the IFHA equivalent circuit of the parallel-type resonant converter with the *LC* filter is given. And the equivalent inductance of FB and CD rectifier circuits is derived.

In order to verify the filter inductor influence of the parallel-type resonant converter, a 500 W PWM–PFM hybrid controlled *LCC* resonant converter is built as a prototype. The close-loop experiment results show the filter inductor may lead to the failure of output voltage regulation and hard-switching operation of power switches. To solve such issues, it is recommended to use IFHA instead of FHA in the parameter design procedure. The accuracy of IFHA is fully demonstrated by the open-loop experiments of the prototype. It is proved that with large filter inductance, the predictions of FHA and IFHA are very close, while with small filter inductance there is a large deviation between the predictions of FHA and IFHA. The experiment results, however, are always accordant with the IFHA predictions, meaning the IFHA successfully describes the influence of the filter inductor in the parallel-type resonant converter.

Appendix

This appendix briefly discusses how to handle the influence of leakage inductance of the power transformer in the parallel-type resonant converter. For parallel-type resonant converters, when the leakage inductance of the transformer is much smaller than resonant inductance, its influence usually can be ignored. However, in some cases where transformer leakage inductance is relatively large, the influence of leakage inductance can be

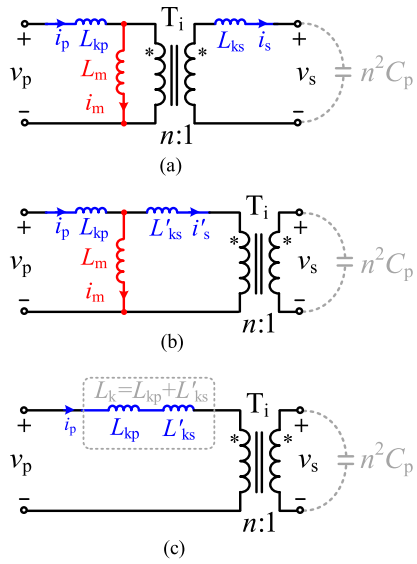

Fig. 16. Equivalent and simplified circuits of the power transformer with the parallel resonant capacitor placed at the secondary side. (a) Equivalent circuit of the power transformer. (b) Equivalent circuit with parasitic parameters reflected to the primary side. (c) Simplified circuit of the power transformer.

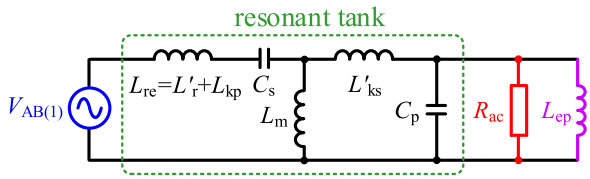

Fig. 17. IFHA equivalent circuits for the *LCC* resonant converter with small magnetizing inductance.

obvious. For such situations, it is recommended to place the parallel resonant capacitor at the secondary side of the power transformer, and the leakage inductance can be absorbed into resonant inductance. The detailed explanation is given below.

Fig. 16 shows the equivalent and simplified circuits of the power transformer. Since the parallel resonant capacitor is placed at the secondary side of the power transformer, its capacitance becomes n^2C_p. The equivalent circuit in Fig. 16(a) takes primary/secondary leakage inductance and magnetizing inductance into consideration. Usually, for the convenience of discussion, L_{sp} is reflected to the primary side, as shown in Fig. 16(b). For most parallel-type resonant converters like PRC or *LCC*, the magnetizing inductance is much larger than leakage inductance, resulting in $i_p \approx i'_s$, and thus, the branch of magnetizing inductance can be ignored, as shown in Fig. 16(c). L_{kp} and L'_{ks} in Fig. 16(c) can be treated as an equivalent inductor L_k, given such L_k is in series connection with resonant inductor L_r, it is absorbed by L_r. Therefore, by placing the parallel resonant capacitor at the secondary side of the power transformer, leakage inductance can be integrated into resonant inductance, and thus, its influence is involved in the IFHA modeling.

Another troublesome situation is that the power transformer has only several primary/secondary turns, where the magnetizing inductance could be small and even comparable with leakage inductance. In such case, the conclusion of $i_p \approx i'_s$ in Fig. 16(b) does not stand anymore, and hence, the secondary leakage in-

ductor L'_{ks} could not be absorbed by resonant inductor L_r, as shown in Fig. 16(c). In order to solve such problem, taking the *LCC* resonant converter as an example, it is suggested to use the equivalent circuit in Fig. 17 instead in Fig. 11(b). As illustrated in Fig. 17, due to the influence of magnetizing inductance L_m and secondary leakage inductance L'_{ks}, the *LCC* resonant tank should be treated as a fifth-order resonant network. However, it should be emphasized that IFHA modeling is still valid in such case, and the expression of L_{ep} is the same as (11) or (21).

REFERENCES

[1] D. Huang, F. C. Lee, and D. Fu, "Classification and selection methodology for multi-element resonant converters," in *Proc. 26th Annu. IEEE Appl. Power Electron. Conf. Expo.*, 2011, pp. 558–565.

[2] R. P. Severns, "Topologies for three-element resonant converters," *IEEE Trans. Power Electron.*, vol. 7, no. 1, pp. 89–98, Jan. 1992.

[3] S. Tian, F. C. Lee, and Q. Li, "A simplified equivalent circuit model of series resonant converter," *IEEE Trans. Power Electron.*, vol. 31, no. 5, pp. 3922–3931, May 2016.

[4] M. M. Ghahderijani, M. Castilla, A. Momeneh, J. T. Miret, and L. G. de Vicuña, "Frequency-modulation control of a dc/dc current-source parallel-resonant converter," *IEEE Trans. Ind. Electron.*, vol. 64, no. 7, pp. 5392–5402, Jul. 2017.

[5] R. Yang, H. Ding, Y. Xu, L. Yao, and Y. Xiang, "An analytical steady state model of LCC type series–parallel resonant converter with capacitive output filter," *IEEE Trans. Power Electron.*, vol. 29, no. 1, pp. 328–338, Jan. 2014.

[6] H. N. Vu and W. J. Choi, "A novel dual full-bridge LLC resonant converter for CC and CV charges of batteries for electric vehicles," *IEEE Trans. Ind. Electron.*, vol. 65, no. 3, pp. 2212–2225, Mar. 2018.

[7] A. K. Rathore, D. R. Patil, and D. Srinivasan, "Non-isolated bidirectional soft-switching current-fed LCL resonant dc/dc converter to interface energy storage in dc microgrid," *IEEE Trans. Ind. Appl.*, vol. 52, no. 2, pp. 1711–1722, Mar./Apr. 2016.

[8] C. Liu, J. Wang, K. Colombage, C. Gould, and B. Sen, "A CLLC resonant converter based bidirectional EV charger with maximum efficiency tracking," in *Proc. 8th IET Int. Conf. Power Electron., Mach. Drives*, Apr. 2016, pp. 1–6.

[9] R. L. Steigerwald, "A comparison of half-bridge resonant converter topologies," *IEEE Trans. Power Electron.*, vol. 3, no. 2, pp. 174–182, Apr. 1988.

[10] Z. Hu, Y. Qiu, L. Wang, and Y. F. Liu, "An interleaved LLC resonant converter operating at constant switching frequency," *IEEE Trans. Power Electron.*, vol. 29, no. 6, pp. 2931–2943, Jun. 2014.

[11] J. Deng, S. Li, S. Hu, C. Mi, and R. Ma, "Design methodology of LLC resonant converters for electric vehicle battery chargers," *IEEE Trans. Veh. Technol.*, vol. 63, no. 4, pp. 1581–1592, May 2014.

[12] M. K. Kazimierczuk and D. Czarkowski, *Resonant Power Converters*. New York, NY, USA: Wiley, 2012.

[13] B. Lu, W. Liu, Y. Liang, F. C. Lee, and J. D. van Wyk, "Optimal design methodology for LLC resonant converter," in *Proc. 21st Annu. IEEE Appl. Power Electron. Conf. Expo.*, 2006, pp. 533–538.

[14] X. Fang, H. Hu, Z. J. Shen, and I. Batarseh, "Operation mode analysis and peak gain approximation of the LLC resonant converter," *IEEE Trans. Power Electron.*, vol. 27, no. 4, pp. 1985–1995, Apr. 2012.

[15] X. Zhao, L. Zhang, R. Born, and J. S. Lai, "A high-efficiency hybrid resonant converter with wide-input regulation for photovoltaic applications," *IEEE Trans. Ind. Electron.*, vol. 64, no. 5, pp. 3684–3695, May 2017.

[16] S. H. Ryu, D. H. Kim, M. J. Kim, J. S. Kim, and B. K. Lee, "Adjustable frequency-duty-cycle hybrid control strategy for full-bridge series resonant converters in electric vehicle chargers," *IEEE Trans. Ind. Electron.*, vol. 61, no. 10, pp. 5354–5362, Oct. 2014.

[17] K. Ali, P. Das, and S. K. Panda, "Analysis and design of APWM half-bridge series resonant converter with magnetizing current assisted ZVS," *IEEE Trans. Ind. Electron.*, vol. 64, no. 3, pp. 1993–2003, Mar. 2017.

[18] X. Sun, X. Li, Y. Shen, B. Wang, and X. Guo, "Dual-bridge LLC resonant converter with fixed-frequency PWM control for wide input applications," *IEEE Trans. Power Electron.*, vol. 32, no. 1, pp. 69–80, Jan. 2017.

[19] N. Harischandrappa and A. K. S. Bhat, "A fixed-frequency LCL-type series resonant converter with a capacitive output filter using a modified gating scheme," *IEEE Trans. Ind. Appl.*, vol. 50, no. 6, pp. 4056–4064, Nov./Dec. 2014.

[20] S. Bhowmick and A. K. S. Bhat, "A fixed-frequency LCC-type resonant converter with inductive output filter using a modified gating scheme," in *Proc. Int. Conf. Adv. Energy Convers. Technol.*, 2014, pp. 140–145.

[21] A. K. S. Bhat, "Fixed-frequency PWM series-parallel resonant converter," *IEEE Trans. Ind. Appl.*, vol. 28, no. 5, pp. 1002–1009, Sep./Oct. 1992.

[22] A. K. S. Bhat, "A generalized steady-state analysis of resonant converters using two-port model and Fourier-series approach," *IEEE Trans. Power Electron.*, vol. 13, no. 1, pp. 142–151, Jan. 1998.

[23] H. Pinheiro, P. K. Jain, and G. Joos, "Self-sustained oscillating resonant converters operating above the resonant frequency," *IEEE Trans. Power Electron.*, vol. 14, no. 5, pp. 803–815, Sep. 1999.

[24] A. J. Forsyth, G. A. Ward, and S. V. Mollov, "Extended fundamental frequency analysis of the LCC resonant converter," *IEEE Trans. Power Electron.*, vol. 18, no. 6, pp. 1286–1292, Nov. 2003.

[25] J. Hou, Q. Chen, X. Ren, X. Ruan, S. Wong, and C. K. Tse, "Precise characteristics analysis of series/series-parallel compensated contactless resonant converter," *IEEE J. Emerging Sel. Topics Power Electron.*, vol. 3, no. 1, pp. 101–110, Mar. 2015.

[26] A. Bucher, T. Duerbaum, D. Kuebrich, and S. Hoehne, "Multi-resonant LCC converter - Comparison of different methods for the steady-state analysis," in *Proc. IEEE Power Electron. Spec. Conf.*, Jun. 2008, pp. 1891–1897.

[27] H. Wang and A. Khaligh, "Comprehensive topological analyses of isolated resonant converters in PEV battery charging applications," in *Proc. IEEE Transp. Electrif. Conf. Expo.*, 2013, pp. 1–7.

[28] J. Biela, U. Badstuebner, and J. W. Kolar, "Impact of power density maximization on efficiency of dc–dc converter systems," *IEEE Trans. Power Electron.*, vol. 24, no. 1, pp. 288–300, Jan. 2009.

[29] G. Ivensky, A. Kats, and S. Ben-Yaakov, "A novel RC model of capacitive-loaded parallel and series-parallel resonant dc-dc converters," in *Proc. IEEE Power Electron. Spec. Conf.*, 1997, vol. 2, pp. 958–964.

[30] S. Gavin, M. Carpita, P. Ecoeur, H. P. Biner, M. Paolone, and E. Talon Louokdom, "A digitally controlled 125 kVdc, 30 kW power supply with an LCC resonant converter working at variable dc-link voltage: Full scale prototype test results," in *Proc. 7th IET Int. Conf. Power Electron., Mach. Drives*, Apr. 2014, pp. 1–6.

[31] A. A. Aboushady, S. J. Finney, B. W. Williams, and K. H. Ahmed, "Steady state analysis of the phase-controlled LCC-type series-parallel resonant converter operating above resonance," in *Proc. 28th Annu. IEEE Appl. Power Electron. Conf. Expo.*, 2013, pp. 2125–2131.

[32] Y. M. Chen, J. P. Xu, J. Cao, L. M. Lin, and H. B. Ma, "PWM–PFM hybrid controlled LCC resonant converter with wide ZVS range and narrow switching frequency variation," *Electron. Lett.*, vol. 53, no. 17, pp. 1218–1220, Aug. 2017.

[33] G. Ivensky, S. Bronstein, and S. Ben-Yaakov, "Approximate analysis of the resonant LCL dc-dc converter," in *Proc. 23rd IEEE Conv. Electr. Electron. Eng. Israel*, 2004, pp. 44–47.

Yiming Chen was born in Sichuan, China, in 1990. He received the B.S. degree in electrical engineering in 2013 from Southwest Jiaotong University, Chengdu, China, where he is currently working toward the Ph.D. degree at the School of Electrical Engineering.

His current research interests include the modeling methods, circuit topologies, and control strategies of a resonant converter.

Jianping Xu (M'10) received the B.S. and Ph.D. degrees in electronic engineering from the University of Electronics Science and Technology of China, Chengdu, China, in 1984 and 1989, respectively.

Since 1989, he has been with the School of Electrical Engineering, Southwest Jiaotong University, Chengdu, China, where he has been a Professor since 1995. From November 1991 to February 1993, he was with the Department of Electrical Engineering, University of Federal Defense Munich, Munich, Germany, as a Visiting Research Fellow. From February 1993 to July 1994, he was with the Department of Electrical Engineering and Computer Science, University of Illinois at Chicago, Chicago, IL, USA, as a Visiting Scholar. His research interests include the modeling, analysis, and control of power electronic systems.

Jin Sha received the B.S. and Ph.D. degrees in electrical engineering from Southwest Jiaotong University, Chengdu, China, in 2009 and 2015, respectively.

From 2013 to 2015, she was a Visiting Researcher with the Department of Electronic and Electrical Engineering, University of Strathclyde, Glasgow, U.K. She was a Research Associate with the University of Strathclyde, during 2016–2017. She is currently an Associate Professor with the School of Electrical Engineering, Southwest Jiaotong University. Her research interests include modeling, analysis, and control of power converters and nonlinear control for renewable power applications.

Leiming Lin was born in Shanxi, China, in 1992. He received the B.S. degree in electrical engineering from North China University of Science and Technology, Tangshan, China, in 2014. He is currently working toward the M.S. degree in electrical engineering at Southwest Jiaotong University, Chengdu, China.

His research interests include the circuit topologies and control strategies of resonant dc–dc converters.

Jing Cao was born in Guangdong, China, in 1992. He received the B.S. degree in electrical engineering in 2015 from Southwest Jiaotong University, Chengdu, China, where he is currently working toward the M.S. degree at the School of Electrical Engineering.

His research interests include the control strategies of the resonant dc–dc converter.